2026 IEEE/SICE International Symposium on System Integration (SII)
January 11-14, 2026. Cancún, México

Modular Vacuum-Based Fixturing System for Adaptive Disassembly Workspace Integration

Haohui Pan[1], Takuya Kiyokawa[1], Tomoki Ishikura[2],
Shingo Hamada[2], Genichiro Matsuda[2], and Kensuke Harada[1]

***Abstract*— The disassembly of small household appliances poses significant challenges due to their complex and curved geometries, which render traditional rigid fixtures inadequate. In this paper, we propose a modular vacuum-based fixturing system that leverages commercially available balloon-type soft grippers to conform to arbitrarily shaped surfaces and provide stable support during screw-removal tasks. To enable a reliable deployment of the system, we develop a stability-aware planning framework that samples the bottom surface of the target object, filters candidate contact points based on geometric continuity, and evaluates support configurations using convex hull-based static stability criteria. We compare the quality of object placement under different numbers and configurations of balloon hands. In addition, real-world experiments were conducted to compare the success rates of traditional rigid fixtures with our proposed system. The results demonstrate that our method consistently achieves higher success rates and superior placement stability during screw removal tasks.**

Index Terms - Disassembly Automation, Soft Robotics, Vacuum-Based Fixturing, Stability-Aware Planning, Small-scale Appliances.

I. Introduction

As demand for sustainable manufacturing and the circular economy grows, robotic disassembly is becoming a key technology for end-of-life product recovery. However, existing systems typically rely on rigid fixtures and predefined trajectories, limiting adaptability to diverse geometries and uncertain contact conditions [1]–[4]. These limitations are especially pronounced for irregular or delicate components that require precise and compliant contact control.

Soft robotics offers an alternative through morphological adaptability, safe interaction, and compliant force distribution. Soft grippers have shown strong performance in handling fragile or non-uniform objects [5]–[7], enabled by mechanisms such as jamming [8], vacuum actuation [9], and modular balloon structures [10]. Recent advances in topology-optimized designs [11] and data-driven grasping [12] have further improved manipulation capability.

Despite these developments, applying soft actuation to disassembly-oriented fixturing remains underexplored. Unlike grasping, disassembly tasks involve asymmetric press–pull forces from tools such as screwdrivers, creating stability and repeatability challenges in cluttered workspaces [13], [14]. While high-level disassembly planning has been studied [4], fixture-level adaptability to geometric uncertainty is still limited.

[1]Department of Systems Innovation, Graduate School of Engineering Science, The University of Osaka, Toyonaka, Osaka, Japan.

[2]Manufacturing Innovation Division, Panasonic Holdings Corporation, 2-7 Matsuba-cho, Kadoma, Osaka, Japan.

To address this gap, we propose a balloon-based adaptive fixturing system composed of suction modules arranged in multi-point configurations. Inspired by adaptive pin arrays [15] and soft jig platforms [16], our method integrates surface completeness evaluation with convex-hull-based stability analysis [17]. A scoring mechanism incorporating local curvature, internal hollowness, and suction feasibility further ranks viable support regions [18]–[20]. This produces stable fixture plans that tolerate geometric uncertainty and tool-induced perturbations.

We assess the system through comparative simulation of two-point and three-point suction configurations and through hardware experiments contrasting the proposed system with a rigid gripper. The analysis focuses on stability under press loads, repeatability of screw removal, and overall suction feasibility.

Overall, this work bridges soft robotic manipulation and adaptive fixturing for automated disassembly, enabling geometry-aware suction planning without relying on custom rigid holders or precision placement.

II. Related Work

A. Mechanically Adaptive Fixtures

Mechanically adaptive fixtures conform to object geometry through physical mechanisms such as shape-memorable pin arrays [15], granular jamming [8], and soft-jig structures [16]. These systems provide compliance and stiffness for handling irregular objects, but are primarily used in assembly tasks. Disassembly introduces asymmetric tool loads and repeated interactions that challenge fixture durability [1], [2]. Traditional fixture-layout optimization for curved objects [21] typically assumes rigid CAD-based contacts. Our work extends this direction by incorporating soft, suction-based contacts into dynamic support planning.

B. Soft Grippers and Suction Mechanisms

Soft grippers leverage material compliance, pneumatic actuation, and distributed contact to achieve adaptive manipulation [5]–[7]. Surveys highlight diverse architectures suited to task-specific requirements [12]. Vacuum-driven designs offer passive conformity and controllable gripping force [9], [10], and recent advances include modular jamming actuators [8], topology-optimized structures [11], and soft–rigid hybrids [7]. However, few systems examine performance under the quasi-static press and pull forces characteristic of disassembly processes.

978-1-6654-5784-2/26/$31.00 ©2026 IEEE

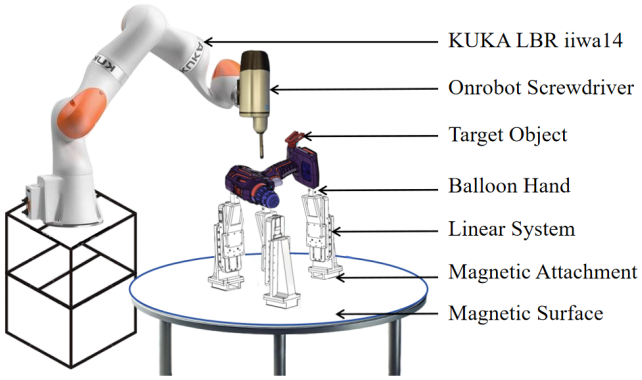

Fig. 1: Overview of the robotic disassembly system consisting of a KUKA LBR iiwa14 arm, Onrobot screwdriver, balloon-hand-based support system, and magnetic attachments for fixture stabilization.

C. Stability and Placement Planning

Grasp stability has been widely studied through contact wrench space, force-closure conditions [18], [22], curvature-based reasoning [19], and actuation-aware robustness [13]. Placement and fixture planning further incorporate geometric or pose uncertainty, which is essential in unstructured disassembly environments [14]. Convex-hull-based analyses [17] and local search approaches [3] provide tractable methods under such uncertainty. Building on these foundations, our work integrates geometric filtering, suction modeling, and force evaluation into a unified stability-aware fixturing pipeline specifically designed for automated screw removal.

III. Proposed Method

A. Assumptions

To support stability analysis and contact planning, several assumptions are made regarding fixture mechanics, object geometry, and the disassembly setup.

Suction forces generated by the balloon-based end-effectors (CONVUM SGB-10[1], shown in Fig. 2) are assumed to act predominantly in the vertical direction, consistent with the quasi-static behavior of vacuum-driven soft actuators under tool weight. Detailed deformation modeling is therefore omitted.

Objects are provided as CAD-based STL models whose bottom surfaces are accessible for ray-based sampling, enabling the system to handle irregular geometries through localized vertical support.

Screw locations and disassembly sequences are predefined. As shown in Fig. 1, the system integrates a KUKA LBR iiwa14 robotic arm, an Onrobot electric screwdriver, and a balloon-hand fixture mounted on a magnetic linear rail, providing stable yet reconfigurable support.

The stability analysis does not assume uniform mass distribution; it only relies on a center-of-mass (COM) estimate from CAD or measurement. As long as the COM is reasonably accurate, the method remains applicable to objects with uneven mass distribution.

Assuming access to a 3D model is realistic for industrial disassembly, where CAD data is usually available. When CAD is unavailable, the pipeline can also operate on reconstructed point-cloud meshes: the ray-casting sampling and coverage filtering inherently tolerate moderate holes and local missing regions, provided that the mesh quality is sufficient.

B. Modular Vacuum-Based System

As shown in Fig. 2, the proposed fixturing system consists of modular vacuum-based end-effectors, each combining a balloon-type soft gripper with an adjustable linear actuator. Every actuator is mounted on a magnetic base for secure attachment to a ferromagnetic table, enabling rapid, reconfigurable deployment without permanent installation. Each module provides compliant vertical support through localized suction and height adjustability, and modules are positioned according to the contact points computed by the planning algorithm. Although placed independently, all modules share a common vacuum source operating at constant suction pressure.

To maintain system simplicity, a minimal-support strategy is used, selecting the fewest modules necessary for stable operation. Preliminary tests showed that single-module setups were unstable, while three-point configurations provided sufficient resistance to displacement and rotation during screw removal.

C. Stability-Based Planning

To enable a reliable deployment of the proposed soft-fixturing system, a four-stage planning framework shown in Fig. 3 is introduced to identify feasible support points: surface sampling, contact completeness filtering, structural continuity filtering, and configuration generation. Initial tests showed that single-module support was insufficient, prompting the adoption of multipoint configurations. The three-point contact sets were ultimately chosen based on stability and feasibility evaluations.

For computational efficiency, each balloon hand is approximated as a point contact at its center during planning. The final candidates are then re-evaluated using full-area suction modeling for accurate force estimation and experimental execution.

Step 1: Support Point Sampling

In Step 1 of Fig. 3, the STL mesh of the target device is assumed to be pre-aligned in a gravity-free pose, meaning that the object is given in a standard CAD coordinate frame rather than its physical resting orientation. This convention is common in CAD modeling and ensures a consistent reference for geometry processing.

The screws are assumed to be approximately perpendicular to the horizontal plane of the robot workspace, reflecting typical consumer-product designs where screws are inserted normal to the main mounting surfaces. This assumption provides a convenient reference for visibility and

[1]https://convum.co.jp/products/en/other-en/sgb/

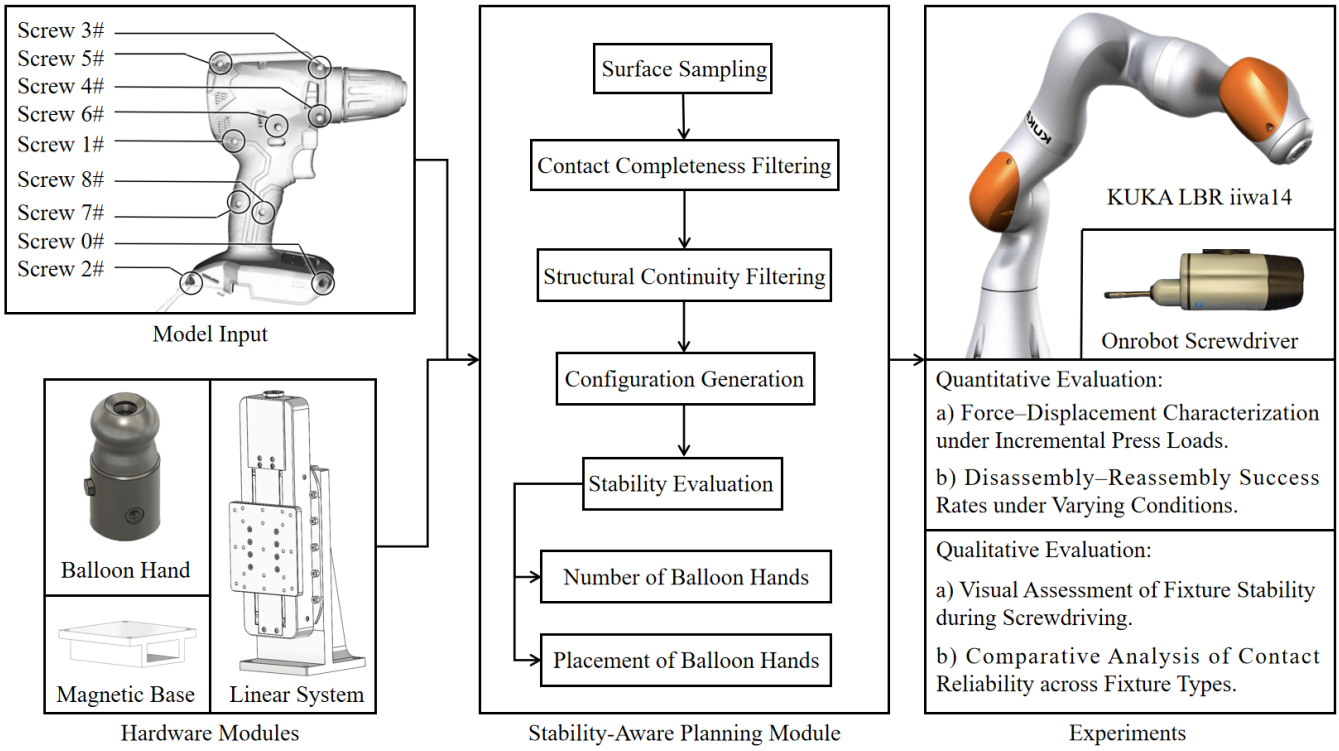

Fig. 2: Overview of the system. The input is an object mesh with annotated screw locations. The stability-aware planning module outputs the number and placement of balloon hands. Experiments validate the results using a robotic screwdriver under quantitative and qualitative criteria.

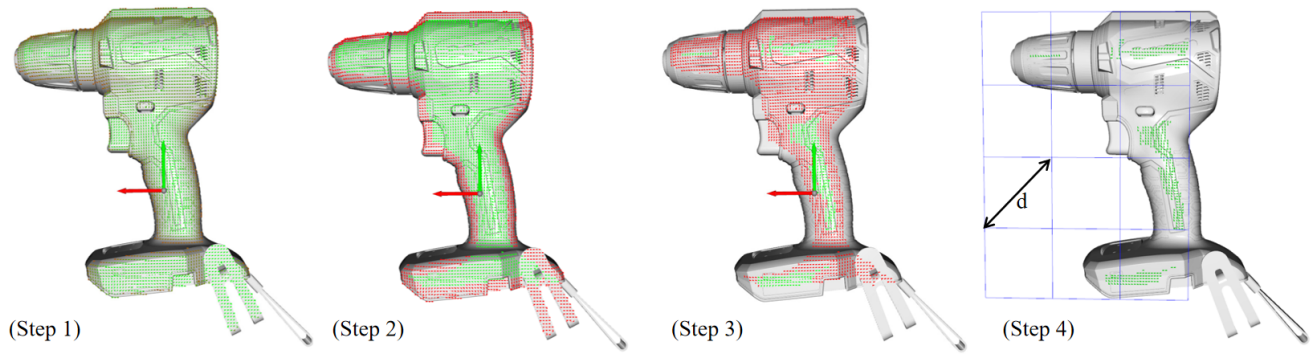

Fig. 3: Support point selection pipeline. Step 1: Surface sampling; Step 2: Contact completeness filtering; Step 3: Structural continuity filtering; Step 4: Configuration generation with spacing constraint ($d = 60\,\mathrm{mm}$). Green points are retained candidates, and red points are those removed due to excessive surface inclination or occlusion in the $-Z$ direction.

tool-orientation constraints, and other orientations can be accommodated by redefining the screw axis if required.

Before describing the candidate sampling process, we briefly introduce the running example: a small consumer electronic enclosure with multiple screws and a moderately curved bottom surface. This object serves solely as an illustration; the method remains applicable to a wide range of geometries and surface conditions.

Surface sampling is performed by casting vertical rays in the $+Z$ direction from a 2 mm-resolution grid over the XY plane. Each ray records all mesh intersections, producing 42,495 initial surface points. We denote this set as P_0. Multiple intersections per ray occur due to internal geometry rather than only external surfaces.

To refine the raw point set, a surface-inclination filter is applied to remove points on highly curved regions. For each point $\mathbf{p}_i \in \mathcal{P}_0$, its nearest $k = 50$ neighbors are collected, and singular value decomposition (SVD) is performed on the centered neighborhood. The surface normal $\mathbf{n}_i$ is taken as the singular vector corresponding to the smallest singular value. The inclination relative to the vertical direction $\mathbf{z}$ is computed as $\angle(\mathbf{n}_i, \mathbf{z})$, and a point is retained only if:

$$\angle(\mathbf{n}_i, \mathbf{z}) \leq 60^\circ. \tag{1}$$

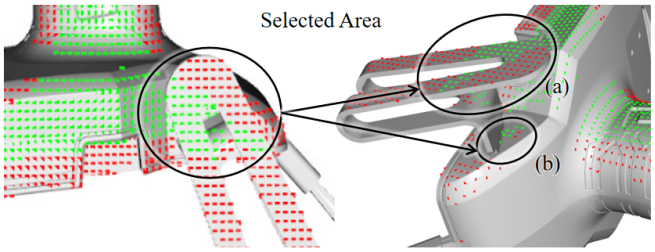

Fig. 4: Contact completeness filtering in Step 2. Area (a) shows points retained due to continuous and well-supported local surfaces, whereas Area (b) shows points rejected due to holes or discontinuities that result in insufficient coverage.

The resulting inclination-filtered set is

$$\mathcal{P}_1 = \{\, \mathbf{p} \in \mathcal{P}_0 \mid \angle(\mathbf{n}_p, \mathbf{z}) \leq 60^\circ \,\}, \tag{2}$$

yielding 32,633 candidates. The 60° threshold is based on preliminary SGB-10 characterization: steeper surfaces caused edge lifting and loss of vacuum sealing, whereas gentler slopes allowed stable contact.

To further refine the candidates, a visibility filter removes points occluded from the $-Z$ direction. Some points in $\mathcal{P}_1$ lie on locally planar regions but are inaccessible due to cavities or overhangs. Visible points are retained as:

$$\mathcal{P}_2 = \{\, \mathbf{p} \in \mathcal{P}_1 \mid \mathrm{vis}_{-\mathbf{z}}(\mathbf{p}) = 1 \,\}, \tag{3}$$

where $\mathrm{vis}_{-\mathbf{z}}(\mathbf{p})$ is a binary visibility indicator evaluated via a ray–casting test. A ray is cast from the $-Z$ direction toward the mesh, and $\mathrm{vis}_{-\mathbf{z}}(\mathbf{p}) = 1$ only if the first surface hit by the ray is point $\mathbf{p}$; otherwise the point is considered occluded and assigned 0. This removes points hidden inside cavities or under overhangs.

Next, to ensure gravitational stability, we discard points located above the plane passing through the object's center of mass $\mathbf{c}_{\text{COM}}$, as such points are prone to tipping and cannot provide stable support:

$$\mathcal{P}_{\text{support}} = \{\mathbf{p} \in \mathcal{P}_2 \mid z_p < z_{\text{COM}}\}. \tag{4}$$

After all filtering stages, a total of 4,099 viable support points remain. These serve as the input to the subsequent contact completeness analysis.

As illustrated in Step 1 of Fig. 3, the final filtered point set provides a geometrically and physically plausible foundation for stability-aware fixture planning in the following stages.

Step 2: Contact Completeness filtering

To ensure that each candidate point can physically accommodate a vacuum-based fixture, we evaluate contact completeness using a geometric surface-coverage criterion derived from the physical constraints of the SGB-10 balloon hand. A suction module requires a locally continuous, hole-free, and sufficiently smooth region to maintain an airtight seal; small cavities or sharp height changes may cause membrane collapse or edge lifting. The completeness criterion therefore enforces that the neighborhood of each point contains a dense and contiguous set of supporting samples consistent with these sealing requirements.

For this criterion, we simulate a ring of suction by casting rays vertically upward along a circle of suction radius $r = 8.7\,\mathrm{mm}$, centered at each candidate point $p \in P_{\text{support}}$. Let $\mathcal{R}(p)$ denote the set of rays sampled along the suction ring, and let $\mathcal{H}(p) \subseteq \mathcal{R}(p)$ denote the subset of rays that intersect the mesh within a short vertical distance above the point. A point is considered to have sufficient surface coverage if:

$$\frac{|\mathcal{H}(p)|}{|\mathcal{R}(p)|} \geq \tau, \quad \text{where } \tau = 0.9. \tag{5}$$

The notation $|\cdot|$ denotes the cardinality of a set, i.e., the number of rays in $\mathcal{R}(p)$ and the number of successful intersections in $\mathcal{H}(p)$. This condition ensures that the local contact region is not disrupted by holes or abrupt height transitions that would compromise vacuum sealing.

The surface-coverage-filtered set is thus defined as:

$$P_3 = \left\{ p \in P_{\text{support}} \,\middle|\, \frac{|\mathcal{H}(p)|}{|\mathcal{R}(p)|} \geq 0.9 \right\}. \tag{6}$$

As shown in Step 2 of Fig. 3, 2,753 contact points were retained after all filtering stages. At this stage, we do not yet consider structural support along the Z-axis. Since candidate points in Step 1 were generated from a 2D projection onto the XY plane, any hollowness or internal gaps directly beneath the contact points cannot be determined here. These structural constraints will be addressed in Step 3.

Step 3: Structural Continuity Filtering

While surface completeness ensures an adequate contact area for sealing, structural continuity beneath each candidate point is also critical to prevent fixture placement in hollow or uneven regions. As illustrated in Fig. 4, many points accepted in Step 2 lie on vertically inconsistent features—e.g., slots, ridges, or embossed patterns—posing risks to suction stability.

To mitigate this, a geometric continuity filter is applied to exclude points on structurally discontinuous surfaces. For each contact point $p \in P_3$, a circular neighborhood $\mathcal{N}(p)$ is defined in the XY plane using the suction radius of the gripper $r = 8.7\,\mathrm{mm}$. The "vertical deviation" of each neighbor is defined as the height difference between the neighbor and the center point. Let z_p denote the z-coordinate of the candidate point p, and let z_q denote the z-coordinate of a neighboring point $q \in \mathcal{N}(p)$. The deviation is computed as

$$\Delta z_q = |z_q - z_p|. \tag{7}$$

Points exceeding a threshold of $\delta = 2.5\,\mathrm{mm}$ are rejected:

$$P_4 = \{\, p \in P_3 \mid \forall\, q \in \mathcal{N}(p),\, \Delta z_q \leq \delta \,\}. \tag{8}$$

As shown in Step 3 of Fig. 3, while projection XY suggests local smoothness, discontinuities in Z remain prevalent near cutouts and embossed features. As illustrated in Fig. 4, green points indicate retained candidates; red points violate the continuity condition. This highlights the need to incorporate vertical consistency for robust fixture planning in real-world geometries.

To enable efficient spatial queries, a 2D k-dimensional tree is constructed from the (x, y) coordinates of the filtered

candidates. Applying the continuity criterion yields 403 viable support points, which are forwarded to the configuration generation stage.

IV. Evaluations

This section evaluates the proposed stability-aware planning pipeline via quantitative simulation and hardware validation. Using the filtered candidates from Step 3, valid two-point (2P) and three-point (3P) support configurations are generated under physical constraints of the balloon-based modules.

A. Configuration Generation and Stability Criteria

As illustrated in Step 4 of Fig. 3, the XY plane is partitioned into a uniform grid whose cell diagonal is $60\,\mathrm{mm}$, corresponding to the effective footprint of a balloon-hand module. This ensures that at most one candidate point is selected per cell, preventing collisions between adjacent modules. The grid does not bias the stability evaluation, since stability depends only on the relative geometry of the support points and the projected center of mass, which is invariant to global translations of the object.

Step 4: Configuration Generation

From the filtered candidates obtained in Step 4, we generate candidate configurations for both two-point (2P) and three-point (3P) setups. Each configuration is required to satisfy a geometric stability condition based on the object's center of mass c_{COM}.

To evaluate the geometric stability of each candidate configuration, we adopt a unified convex hull-based inclusion criterion that explicitly accounts for the circular footprint of the suction cups.

Each suction contact point is modeled as a circular region of radius $r = 8.7\,\mathrm{mm}$. For each point p_i, we generate two auxiliary points by offsetting along the direction orthogonal to the local support plane (typically the XY plane). The set of all offset points is defined as:

$$\mathcal{V} = \bigcup_i \{p_i + r \cdot \mathbf{n}_i,\ p_i - r \cdot \mathbf{n}_i\}\,, \tag{9}$$

where $\mathbf{n}_i$ denotes the unit normal vector orthogonal to the baseline at p_i. The resulting expanded support footprint used for convex-hull evaluation is illustrated in Fig. 5. This convex-hull-based stability check naturally eliminates collinear or nearly collinear triplets, since such configurations form a degenerate support region that cannot contain the center of mass.

This convex-hull inclusion criterion is motivated by static equilibrium considerations. When the object's center of mass lies strictly within the convex polygon formed by the suction contact region, there exists a set of positive support forces $\{\mathbf{f}_i\}$ such that both force and moment balance are satisfied under gravity:

$$\sum_i \mathbf{f}_i + \mathbf{f}_g = \mathbf{0}, \quad \sum_i (\mathbf{p}_i - \mathbf{c}_{\text{COM}}) \times \mathbf{f}_i = \mathbf{0}, \tag{10}$$

where $\mathbf{f}_g$ is the gravitational force acting at the center of mass. The existence of such a solution implies that the configuration is capable of resisting tipping or rotation under gravitational loading.

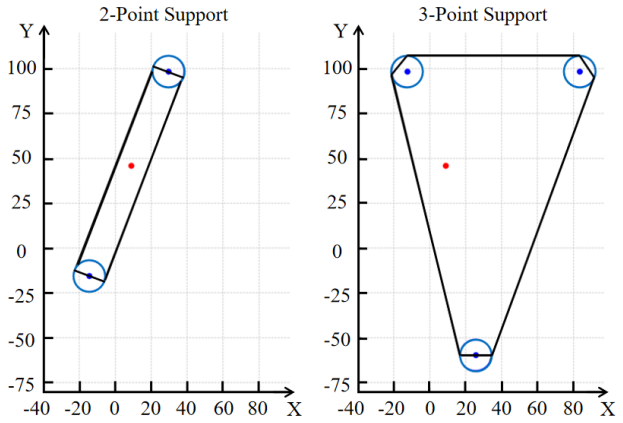

Fig. 5: Visualized support configurations on the XY plane. Blue dots indicate the balloon hand contact points; the red dot denotes the object's center of mass.

Therefore, as shown in Fig. 5, the inclusion test $\mathbf{c}_{\text{COM}} \in \text{ConvexHull}(\mathcal{V})$ serves as a sufficient geometric condition for potential static stability in the 2D projected support plane.

B. Stability Analysis of Support Configurations

To ensure that candidate support configurations can stably hold the object during disassembly, we evaluate their resistance to external forces using a static equilibrium framework. Although dynamic simulation could model time-dependent effects, it requires detailed contact and material parameters that are difficult to estimate reliably. A quasistatic formulation is therefore adopted to capture the dominant failure modes—primarily tipping and slipping—while keeping the analysis simple and robust.

1) Static Equilibrium Model: We first assess whether each candidate support configuration can maintain static equilibrium when the object is initially placed onto the support structure. The external forces considered include gravity and a constant downward press force applied by the screwdriver upon contact. For each n-point support configuration $\{p_j\}_{j=1}^n$, we extract the local surface normals $\{\mathbf{n}_j\}$ from the mesh and define the moment arms $\mathbf{r}_j = p_j - \mathbf{c}_{\text{COM}}$, where $\mathbf{c}_{\text{COM}}$ is the object's center of mass. The static equilibrium system is written as:

$$\underbrace{\begin{bmatrix} \mathbf{n}_1^\top \\ \mathbf{n}_2^\top \\ \vdots \\ \mathbf{n}_n^\top \\ (\mathbf{r}_1 \times \mathbf{n}_1)^\top \\ (\mathbf{r}_2 \times \mathbf{n}_2)^\top \\ \vdots \\ (\mathbf{r}_n \times \mathbf{n}_n)^\top \end{bmatrix}}_{A \in \mathbb{R}^{6\times n}} \cdot \underbrace{\begin{bmatrix} f_1 \\ f_2 \\ \vdots \\ f_n \end{bmatrix}}_{\mathbf{F} \in \mathbb{R}^{n\times 1}} = \underbrace{\begin{bmatrix} 0 \\ 0 \\ -mg - f_{\text{press}} \\ 0 \\ 0 \\ 0 \end{bmatrix}}_{\mathbf{b} \in \mathbb{R}^{6\times 1}} \tag{11}$$

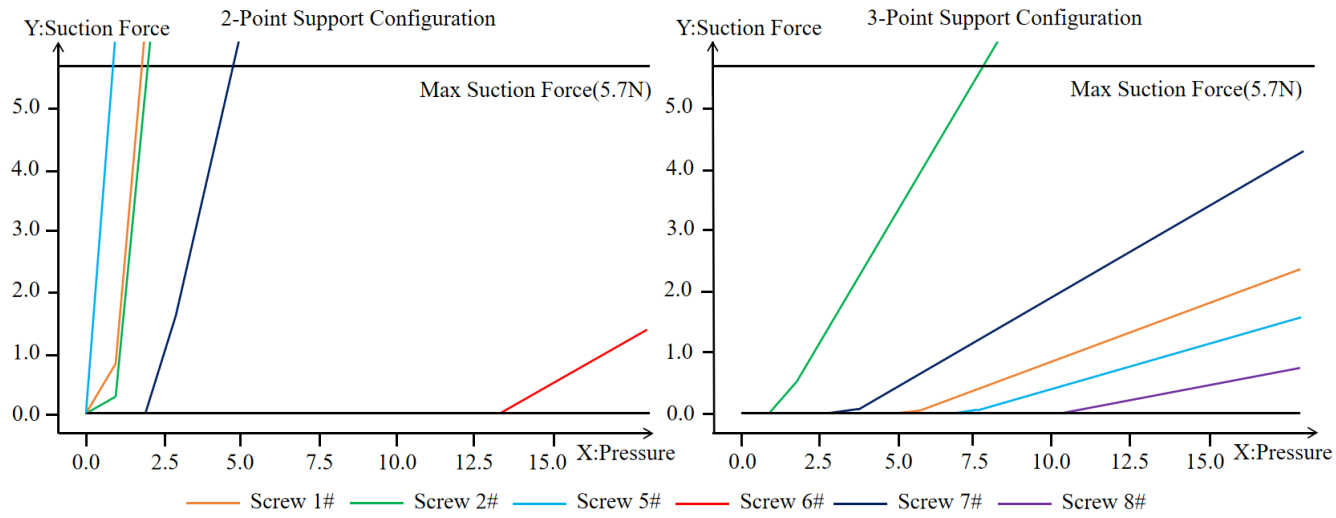

Fig. 6: Required suction force per balloon under increasing press force for different screws. The X-axis represents the linearly increased disassembly press force applied by the screwdriver. The Y-axis indicates the corresponding suction force required to maintain equilibrium.

The normal contact force computed f_i at each support point is not constrained to be non-negative. If $f_i < 0$, it implies that suction is required to maintain equilibrium. As long as the suction demand satisfies

$$f_i \geq -f_{\max}, \tag{12}$$

where $f_{\max} = 5.7\,\mathrm{N}$ denotes the suction limit of a single balloon contact, the configuration remains feasible.

TABLE I: Pull/Push Forces for Each Screw under 2-Point (2P) and 3-Point (3P) Support

Screw	**2P Configuration** [N]		**3P Configuration** [N]		
	Balloon 1	Balloon 2	Balloon 1	Balloon 2	Balloon 3
0	262.05	280.94	2.37	21.12	6.21
1	-6.10	-7.02	23.86	8.19	-2.35
2	-1.50	-5.78	14.29	12.26	-6.33
3	35.13	67.19	14.64	1.59	13.48
4	86.38	115.03	11.88	6.14	11.68
5	-6.80	-6.95	30.30	0.96	-1.55
6	-1.51	6.50	17.65	7.00	5.06
7	-2.18	-6.37	19.75	14.22	-4.27
8	48.05	41.69	15.42	15.02	-0.74

2) Quantitative Force Evaluation: As summarized in Table I, the required push and pull forces at each screw location are computed from the spatial arrangement of support points. A linearly increasing press force is applied, and negative values in Table I represent the suction force needed to maintain equilibrium. When this demand exceeds the balloon hand's maximum capacity (5.7 N), the screw is deemed unstable.

In the 2-point configuration, screws #1, #2, and #5–#7 exceed the suction limit at roughly 2.5 N of applied force (Fig. 6), while screw #6 remains stable up to 17.5 N. In the 3-point configuration, several screws also require higher suction forces, but only screw #2 surpasses the limit, and only above 7.5 N, reflecting improved load distribution.

Screws #0 and #2 are excluded from real-world success-rate tests because their unusually deep screw holes cause simulation and engagement uncertainty.

Although 2-point (2P) configurations satisfy static equilibrium mathematically, they often fail in practice due to poor moment resistance. When a screw is far from the line between the two contacts, the resulting moment generates extremely large reaction forces (e.g., 262.05 N and 280.94 N for screw #0 and #4), far beyond suction capacity. This highlights the inherent limitation of 2P support and the necessity of 3-point (3P) configurations for reliable spatial force closure.

3) Force Evolution Under Increasing Press Load: System behavior during screwdriving is evaluated via a quasi-static simulation, where the applied press force is linearly increased from 0N to 18N. At each increment, static equilibrium is solved and the resulting pull force at each support is examined. Configurations are classified as unstable if any pull force exceeds the suction limit of 5.7N. This procedure offers a tractable means of approximating stability boundaries without resorting to time-dependent modeling.

Force trajectories and final distributions, visualized in Fig. 6, reveal load-sharing patterns and potential risks of overloading individual contacts. The comparison elucidates the mechanical advantages of 3P over 2P support configurations under increasing press loads.

V. Experiments

To validate the feasibility and robustness of the proposed disassembly system, hardware experiments were conducted on real-world screw removal. Before presenting the results, we summarize the experimental setup.

Fig. 7: Disassembly of Screws 1# and 3#–8#. Blue: Initial screwdriver position; Green: Successful disassembly.

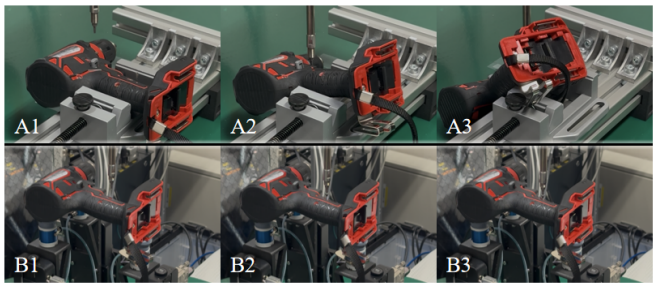

Fig. 8: (A1–A3) Disassembly using a traditional rigid gripper. (B1–B3) Disassembly cycle using our proposed system. The screwdriver loosens the screw from B1 to B2 and retightens it from B2 to B3 without re-alignment.

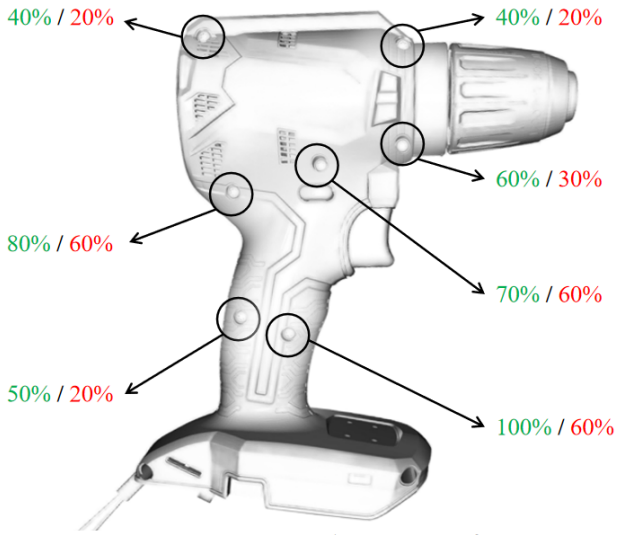

Fig. 9: Success rates of disassembly–reassembly cycles for each screw location under two vertical press forces. Green indicates the success rate under 18 N, and red indicates the success rate under 25 N; the colors correspond to the two separate experimental conditions and do not imply a single-sided threshold.

In the current prototype, the object is manually aligned with the balloon-hand fixture: the operator places the device so that the three suction modules fully contact the selected support points, after which vacuum pressure secures the object. The same alignment procedure is reproduced in Gazebo to simulate the real disassembly environment.

For tool orientation, the screwdriver approaches each screw along its estimated screw axis, assumed perpendicular to the local mounting surface. The robot and object coordinate frames are aligned using two reference points measured on the object in both hardware and Gazebo, enabling consistent approach paths for all disassembly trials.

A. *Feasibility Evaluation of the Disassembly System*

To verify the feasibility of the proposed disassembly approach, single-pass disassembly trials were performed on all seven target screws. As shown in Fig. 7, screws #1 and #3–#8 were successfully removed using the integrated system combining balloon-hand support and the OnRobot screwdriver. In each trial, the robot aligned the tool to the target screw (blue), executed the removal, and success was confirmed by visual extraction (green). These results demonstrate that the integrated support–disassembly workflow is effective under realistic conditions.

For comparison, the same task was executed using a rigid parallel gripper as the support mechanism. As shown in Fig. 8, during the A1–A3 sequence, the object clamped by rigid fingers tends to tilt or slip due to predominantly line or surface contacts, which provide limited constraint and are easily disturbed. Once equilibrium is lost, instability propagates quickly. In contrast, the proposed balloon-hand fixture offers localized suction and geometric conformity, maintaining stable contact and enabling reliable screw loosening and tightening.

B. *Cycle Repeatability Under Varying Press Forces*

This subsection describes the experimental procedure and quantitative evaluation of cycle repeatability under different press forces, while the following subsection (V.C) analyzes the resulting success-rate trends and their mechanical causes.

A repeated disassembly–reassembly test was conducted to evaluate system stability. After initial alignment, the screwdriver performed a full disassembly followed by immediate re-tightening of the same screw, without re-alignment between cycles. Each screw was tested for up to ten repetitions,

and repeatability was measured by the number of successful cycles.

The effect of vertical press force was examined under two loading conditions, 18 N and 25 N. For each condition, repeated cycles were executed to assess the system's tolerance to press-force variation, as shown in Fig. 9.

C. Disassembly Success Rate Analysis

As shown in Fig. 9, the 18 N condition yields success rates above 60% for all screws, whereas 25 N causes a clear degradation. Two effects explain this trend. First, screws closer to the center of mass tolerate larger press forces due to better load distribution. Second, higher press force reduces alignment tolerance: at 18 N, the screwdriver can still self-correct minor misalignments during engagement, but at 25 N the tool descends too rapidly, increasing the likelihood of lateral offset.

Screws near the object boundary are particularly prone to failure, as even small angular deviations cause the screwdriver to slip along the outer surface instead of engaging the screw slot, leading to unsuccessful disassembly.

VI. Conclusion and Future Work

This paper presented a modular vacuum-based fixturing system for stable and repeatable disassembly of irregular objects. The proposed planning framework identifies feasible support configurations through geometric filtering and convex-hull-based stability analysis. Both simulation and hardware experiments demonstrated the feasibility and robustness of the approach across different screw locations and press-force conditions, highlighting the advantages of soft, adaptive support over traditional rigid fixtures.

Future work includes automatic selection of balloon-hand parameters based on estimated contact areas, as well as modeling partial balloon deformation rather than assuming full conformity. Integrating vision-based recognition during disassembly is also planned to improve contact localization and adaptive support adjustment.

Acknoledgement

This work was supported by the New Energy and Industrial Technology Development Organization (NEDO) project JPNP23002.

References

[1] M. Chang, S. Ong, and A. Nee, "Approaches and challenges in product disassembly planning for sustainability," *Procedia Cirp*, vol. 60, pp. 506–511, 2017.

[2] D. Lee, J. Kang, and P. Xirouchakis, "Disassembly planning and scheduling: review and further research," *Proceedings of the Institution of Mechanical Engineers, Part B: Journal of Engineering Manufacture*, vol. 215, no. 5, pp. 695–709, 2001.

[3] Y. Tang, M. Zhou, and R. J. Caudill, "An integrated approach to disassembly planning and demanufacturing operation," *IEEE Transactions on Robotics and Automation*, vol. 17, no. 6, pp. 773–784, 2001.

[4] H. Wang, D. Xiang, Y. Rong, and L. Zhang, "Intelligent disassembly planning: a review on its fundamental methodology," *Assembly Automation*, vol. 33, no. 1, pp. 78–85, 2013.

[5] G. B. Crowley, X. Zeng, and H.-J. Su, "A 3d printed soft robotic gripper with a variable stiffness enabled by a novel positive pressure layer jamming technology," *IEEE Robotics and Automation Letters*, vol. 7, no. 2, pp. 5477–5482, 2022.

[6] S. Dontu, E. Kanhere, T. Stalin, A. G. Dharmawan, C. Hegde, J. Su, X. Chen, S. Magdassi, G. S. Soh, and P. Valdivia Y. Alvarado, "Applications of a vacuum-actuated multi-material hybrid soft gripper: lessons learnt from robosoft manipulation challenge," *Frontiers in Robotics and AI*, vol. 11, p. 1356692, 2024.

[7] A. Gafer, D. Heymans, D. Prattichizzo, and G. Salvietti, "The quad-spatula gripper: A novel soft-rigid gripper for food handling," in *Proceedings of IEEE international conference on soft robotics (RoboSoft)*. IEEE, 2020, pp. 39–45.

[8] Y. Li, Y. Chen, Y. Yang, and Y. Wei, "Passive particle jamming and its stiffening of soft robotic grippers," *IEEE Transactions on robotics*, vol. 33, no. 2, pp. 446–455, 2017.

[9] F. Gabriel, M. Fahning, J. Meiners, F. Dietrich, and K. Dröder, "Modeling of vacuum grippers for the design of energy efficient vacuum-based handling processes," *Production Engineering*, vol. 14, no. 5, pp. 545–554, 2020.

[10] Y. Kemmotsu, K. Tadakuma, K. Abe, M. Watanabe, and S. Tadokoro, "Balloon pin-array gripper: two-step shape adaptation mechanism for stable grasping against object misalignment," *IEEE Robotics and Automation Letters*, 2024.

[11] J. Pinskier, X. Wang, L. Liow, Y. Xie, P. Kumar, M. Langelaar, and D. Howard, "Diversity-based topology optimization of soft robotic grippers," *Advanced Intelligent Systems*, vol. 6, no. 4, p. 2300505, 2024.

[12] Z. Samadikhoshkho, K. Zareinia, and F. Janabi-Sharifi, "A brief review on robotic grippers classifications," in *Proceedings of IEEE Canadian Conference of Electrical and Computer Engineering*. IEEE, 2019, pp. 1–4.

[13] Z. Hu, W. Wan, K. Koyama, and K. Harada, "Reducing uncertainty using placement and regrasp planning on a triangular corner fixture," *IEEE Transactions on Automation Science and Engineering*, vol. 21, no. 1, pp. 652–670, 2023.

[14] P. Nadeau and J. Kelly, "Stable object placement planning from contact point robustness," *IEEE Transactions on Robotics*, 2025.

[15] P. Shi, Z. Hu, K. Nagata, W. Wan, Y. Domae, and K. Harada, "Development of a shape-memorable adaptive pin array fixture," *Advanced Robotics*, vol. 35, no. 10, pp. 591–602, 2021.

[16] T. Kiyokawa, T. Sakuma, J. Takamatsu, and T. Ogasawara, "Soft-jig-driven assembly operations," in *Proceedings of IEEE International Conference on Robotics and Automation (ICRA)*. IEEE, 2021, pp. 3466–3472.

[17] S. Meeran and A. Share, "Optimum path planning using convex hull and local search heuristic algorithms," *Mechatronics*, vol. 7, no. 8, pp. 737–756, 1997.

[18] Y. Funahashi, T. Yamada, M. Tate, and Y. Suzuki, "Grasp stability analysis considering the curvatures at contact points," in *Proceedings of IEEE International Conference on Robotics and Automation (ICRA)*, vol. 4. IEEE, 1996, pp. 3040–3046.

[19] T. Yamada, T. Ooba, T. Yamamoto, N. Mimura, and Y. Funahashi, "Grasp stability analysis of two objects in two dimensions," in *Proceedings of IEEE International Conference on Robotics and Automation (ICRA)*. IEEE, 2005, pp. 760–765.

[20] M. Pozzi, M. Malvezzi, and D. Prattichizzo, "On grasp quality measures: Grasp robustness and contact force distribution in underactuated and compliant robotic hands," *IEEE Robotics and Automation Letters*, vol. 2, no. 1, pp. 329–336, 2016.

[21] D. Ding, G. Xiang, Y.-H. Liu, and M. Y. Wang, "Fixture layout design for curved workpieces," in *Proceedings of IEEE International Conference on Robotics and Automation*, vol. 3. IEEE, 2002, pp. 2906–2911.

[22] G. Liu, J. Xu, X. Wang, and Z. Li, "On quality functions for grasp synthesis, fixture planning, and coordinated manipulation," *IEEE Transactions on Automation Science and Engineering*, vol. 1, no. 2, pp. 146–162, 2004.